ARL-TR-8706 ● JUNE 2019

DEVCOM ARMY RESEARCH LABORATORY

Concept for Spatial Visualization of Magnetic Fields from Exploding Wires

by MB Zellner, R Doney III, WC Uhlig, P Berning, P Bartkowski, and S Halsey

NOTICES

Disclaimers

The findings in this report are not to be construed as an official Department of the Army position unless so designated by other authorized documents.

Citation of manufacturer's or trade names does not constitute an official endorsement or approval of the use thereof.

Destroy this report when it is no longer needed. Do not return it to the originator.

ARL-TR-8706 ● JUNE 2019

Concept for Spatial Visualization of Magnetic Fields from Exploding Wires

by MB Zellner, R Doney III, WC Uhlig, P Berning, P Bartkowski, and S Halsey
Weapons and Materials Research Directorate, CCDC Army Research Laboratory

REPORT DOCUMENTATION PAGE

Form Approved
OMB No. 0704-0188

1. REPORT DATE *(DD-MM-YYYY)*	2. REPORT TYPE	3. DATES COVERED (From - To)
June 2019	Technical Report	1 January–30 April 2019

4. TITLE AND SUBTITLE
Concept for Spatial Visualization of Magnetic Fields from Exploding Wires

5a. CONTRACT NUMBER

5b. GRANT NUMBER

5c. PROGRAM ELEMENT NUMBER

6. AUTHOR(S)
MB Zellner, R Doney III, WC Uhlig, P Berning, P Bartkowski, and S Halsey

5d. PROJECT NUMBER

5e. TASK NUMBER

5f. WORK UNIT NUMBER

7. PERFORMING ORGANIZATION NAME(S) AND ADDRESS(ES)
US Army Combat Capabilities Development Command Army Research Laboratory
ATTN: FCDD-RWL-PD
Aberdeen Proving Ground, MD 21005

8. PERFORMING ORGANIZATION REPORT NUMBER
ARL-TR-8706

9. SPONSORING/MONITORING AGENCY NAME(S) AND ADDRESS(ES)

10. SPONSOR/MONITOR'S ACRONYM(S)

11. SPONSOR/MONITOR'S REPORT NUMBER(S)

12. DISTRIBUTION/AVAILABILITY STATEMENT
Approved for public release; distribution is unlimited.

13. SUPPLEMENTARY NOTES
ORCID IDs: MB Zellner, 0000-0001-7309-312X; WC Uhlig, 0000-0003-1815-0106; P Berning, 0000-0001-9699-0245

14. ABSTRACT
The US Army Combat Capabilities Development Command Army Research Laboratory is interested in how EM fields couple with materials during dynamic events. In this work, we propose a novel method to spatially visualize magnetic fields in situ during dynamic exploding wire experiments for direct comparison with magnetohydrodynamic simulations and to identify where the current is flowing in complex pulsed power experiments. The technique involves characterizing exploding wire experiments simultaneously with X-radiography to inform about the wire's structural location and proton radiography that is sensitive to contributions from both the structural and magnetic field contributions. The data will allow for an inference of where the magnetic fields permeate under the dynamic event and where the preferred conduction paths are located. This proposal was accepted by Los Alamos National Laboratory's (LANL's) proton radiography advisory committee, and experiments will be conducted during the summer of 2020 at LANL's proton radiography facility.

15. SUBJECT TERMS
proton radiograph, X-ray radiography, magnetic field, exploding wire, capacitor, electricity

16. SECURITY CLASSIFICATION OF:			17. LIMITATION OF ABSTRACT	18. NUMBER OF PAGES	19a. NAME OF RESPONSIBLE PERSON
a. REPORT	b. ABSTRACT	c. THIS PAGE			MB Zellner
Unclassified	Unclassified	Unclassified	UU	32	19b. TELEPHONE NUMBER (Include area code) (410) 306-2585

Standard Form 298 (Rev. 8/98)
Prescribed by ANSI Std. Z39.18

Contents

List of Figures

List of Tables

1. Introduction

This work seeks to directly address Army protection problems via validation of current Department of Energy, Department of Defense, and academic computational platforms including multiphysics codes such as ALEGRA[1] and ALE-3D.[2] Additionally, the new experimental technique outlined, which utilizes proton radiography (PRad), will give further insight into theory while identifying, maturing, and developing experimental capabilities regarding pulsed power applications.

The US Army Combat Capabilities Development Command (CCDC) Army Research Laboratory (ARL) is interested in how electromagnetic (EM) fields couple with materials during dynamic events. Because EM entities are often difficult to measure in applicable experiments, researchers utilize multiphysics simulation to help understand their evolution and interactions. These tools are tasked with the difficulty of linking a series of processes and independently confirmed models together to produce an end result. Code validation is required on each piece of the process as well as the combined product to eliminate compounding errors and oversights that cause a noticeable difference in the output. In this work, we propose a novel method to spatially visualize magnetic fields in situ during dynamic events for direct comparison with magnetohydrodynamic (MHD) simulations and identify where the current is flowing in complex pulsed power experiments. These unique experiments have the potential to supply much needed validation to simulations of complex, many entity systems and potentially assess the validity of the following issues and assumptions embedded within current implementations:

- How does the magnetic field evolve in a dynamic environment including fragmentation and vaporization?
- How accurate are conduction/material models as currently implemented, and how does their accuracy/inaccuracy influence the end result when simulating scenarios with extreme stresses and high EM potentials?
- How applicable are approximations used to integrate MHD methods with structural mechanics codes, such as use of an average conductivity in a mixed material cell?

2. Proposed Concept

To spatially visualize magnetic fields and their coupling to matter within a dynamic event, we propose a technique to investigate exploding wires in which

X-radiography and PRad are fielded simultaneously, as in Fig. 1. Such experiments, examples of which are detailed in Table 1, would use capacitive-based pulsed electrical discharge to explode copper wires, generating unique environments in which matter is accelerated, deforms, and fails while being subject to large electrical currents and changing magnetic fields. While exploding wires have undergone extensive studies,[3] they are still of interest in various scientific areas,[4] and the simplicity and enhanced control of exploding (and energized nonexploding) wire experiments allows probing of variables with great independence. These experiments will also allow collection of experimental data from situations where closed-form EM-field solutions exist, which will be useful for validating the experimental technique itself.

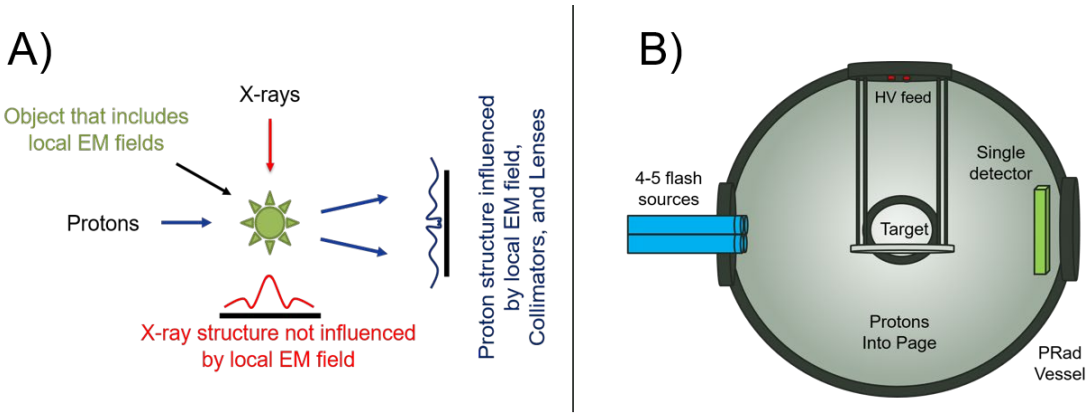

Fig. 1 A) Schematic of proposed experimental setup used to spatially visualize magnetic fields, and B) schematic representation of diagnostic arrangement within the PRad vessel

Table 1 Potential experiments to be conducted

Experiment	Exploding or energized	Information	Material position	Magnetic field
Wire (straight)	Energized	Baseline	Known, X-ray, PRad	Closed-form, ALEGRA, PRad
Wire (straight, 45°)	Energized	Baseline alternate view	Known, X-ray, PRad	Closed-form, ALEGRA, PRad
Tube (straight)	Energized	Modulated baseline	Known, X-ray, PRad	Closed-form, ALEGRA, PRad
Wire (straight)	Exploding	EM field/particle coupling	X-ray, ALEGRA	ALEGRA,PRad
Wire (straight, 45°)	Exploding	EM field/particle coupling	X-ray, ALEGRA	ALEGRA, PRad

Table 1 Potential experiments to be conducted (continued)

Experiment	Exploding or energized	Information	Material position	Magnetic field
Wire (insulated)	Exploding	Insulating particles	X-ray, ALEGRA	ALEGRA, PRad
Wire (heli-coil)	Energized	Complex field	Known, X-ray, PRad	ALEGRA, PRad
Wire (heli-coil)	Exploding	Complex field	X-ray, ALEGRA	ALEGRA, PRad

The ability to observe and separate the materialistic and EM contributions within these experiments stems from utilizing two different media by which transmission radiography will be performed: neutral X-ray photons for the X-radiography and positively charged protons for the proton-radiography. Figure 1A schematically depicts the proposed scheme. For X-ray photons of energy less than 1 MeV, the predominant scattering mechanisms are largely coupled to the electronic density of the atoms that compose the sample, and attenuation of the photons can be closely approximated using the Beer–Lambert law. The neutrality of photons as scattering medium imply that the incident, scattered photons, and nonscattered photons will propagate in a ballistic manner in the presence of large EM fields and will be insensitive to a static or dynamically changing EM field. Therefore, in this setup, X-radiography will be used to ascertain the material's spatial orientation (position).

In the absence of external EM fields, PRad performs a similar task to that of transmission X-radiography, but uses positively charged protons as its scattering medium. Like X-radiography, proton-based scattering interactions relate information linked to the position of the material's atoms within the experimental field of view. However, because the protons are charged, their trajectories are affected by EM fields, and any influence from an EM field present within the target will act as a distortion added to the material-based image. If X-ray and PRad are fielded simultaneously for targets that include an EM field, we could use the EM-influenced proton radiography image in conjunction with the non-EM-influenced X-ray radiograph to infer information about the magnetic field.

In the case of Los Alamos National Laboratory's 800-MeV proton accelerator, the Lorentz force required to shift a proton by 1 milliradian requires an orthogonal 0.1054-T uniform magnetic field over a length of 50 mm. To get a similar deviation via the electric field would require a 26.6-MV/m field 50 mm in length. These

calculations paired with knowledge of the fields attainable during armor and/or exploding wire experiments indicate we should focus on contributions from the magnetic field, and those from the electric field will be negligible. To better visualize the influence of a magnetic field on 800-MeV protons, a Matlab script was composed that traces proton trajectories through a 120- × 120- × 120-mm volume permeated by a magnetic field. Figure 2 depicts how protons would deflect in this region from the magnetic field generated by a wire with 200-kA current. In this case we could expect some 800-MeV protons to deflect many millimeters, which is well above the instrument's current spatial resolution.

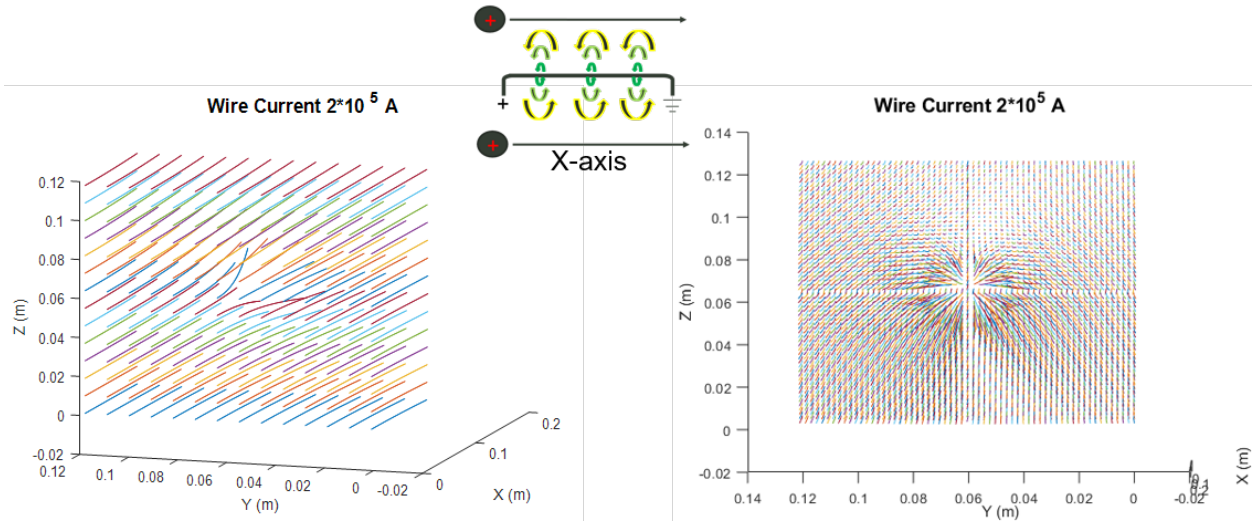

Fig. 2 Proton trajectories (colored lines) for 800-MeV protons traversing the magnetic field generated by a wire conducting 200 kA; (center top) schematic representation of the wire, its magnetic field, and the initial proton direction

To field the proposed experiments and achieve our goals, X-radiography and a high-voltage capacitive driver must be integrated into the PRad vessel. Figure 1B depicts a schematic of the proposed topology.* In this scheme, multiple X-ray sources and a single detector would be used to collect five X-ray snapshots throughout the dynamic event. The L-3 X-ray sources have pulse durations of 40–80 ns and can be triggered to discharge within 500-ns jitter, making synchronization with the PRad proton pulses feasible. To create X-radiographs from a similar viewpoint, we would apply a point spread function correction routine to account for X-ray projection.[5] In the proposed experimental geometry, off-center X-radiographs would incur minimal rotational error (0.667% of the shift length). This error is well below the expected deviation induced to the protons by the

* ARL has already been in communication with various members of the PRad team to assess feasibility. ARL is willing to partner with the PRad team to incorporate these capabilities as well as supply items such as X-ray sources, vessel lids, and pulse power drivers for use during the experiments.

magnetic field, allowing the overall technique to map a high-fidelity comparison from the center X-ray channel and changes in the magnetic field throughout time using the outer channels.

The first proposed experiments to prove this PRad capability would consist of monitoring an energized, but not exploding, wire and tube within the PRad field of view. Although Lorentz forces may induce some movement, these problems will not incur fracture and therefore serve as ideal test problems with well-known geometries and a closed-form magnetic field solution. Additionally, PRad images collected with and without EM fields will allow the mathematics to be confirmed and validate the technique. Following experiments could then move to targets of increased particle distribution and magnetic field complexity, including exploding wires, exploding wires with prepositioned notches intended to control the particle distribution, exploding wires encapsulated in insulators to identify how insulating material can influence the conduction paths, and static and exploding heli-coils in which the complexity of the magnetic field geometry significantly increases.

3. Proof-of-Principle Experiments

Proof-of-principle experiments to inject the capacitive electrical pulse into the PRad vessel and to the wire load have been demonstrated at ARL. Details pertaining to these benchtop exploding wire experiments can be found in Appendix A, and those for a corresponding simulation using ALEGRA can be found in Appendix B. To attain required amperage within the wire for explosion (approximately 200 kA for a 14AWG copper wire with a 10- to 15-μs rise-time), a 190-μf, 20-kV, 38-kJ capacitor bank couples the energy to the load via low-inductance leads and a spark gap switch. Wire explosions occurred with a system jitter below 1 μs, which is sufficient for the proposed experiments. The setup also tested a custom low-inductance high-voltage feed-through, which mimicked that which would be required in a port of a PRad vessel.

The potential for these experiments as a validation technique for addressing our research questions and improving confidence of simulations relating conduction within a changing particle field can be inferred from Fig. 3, which depicts the complex environment of an exploding wire and the sensitivity of the magnetic field to the global material/electronic environment. This figure shows simulations of density and the magnetic field, along with experimentally acquired radiography and photography of exploding wires at different stages throughout its evolution. The simulations compare a pristine wire with one in which the density was randomly perturbed by 1% within its bulk. In the density modulated case, gradients induce local conduction paths within the wire, which ultimately develop into pinch points

and cause asymmetric failure along the wire's length. This appears to be a better representation (compared with experiments) than using a pristine wire.

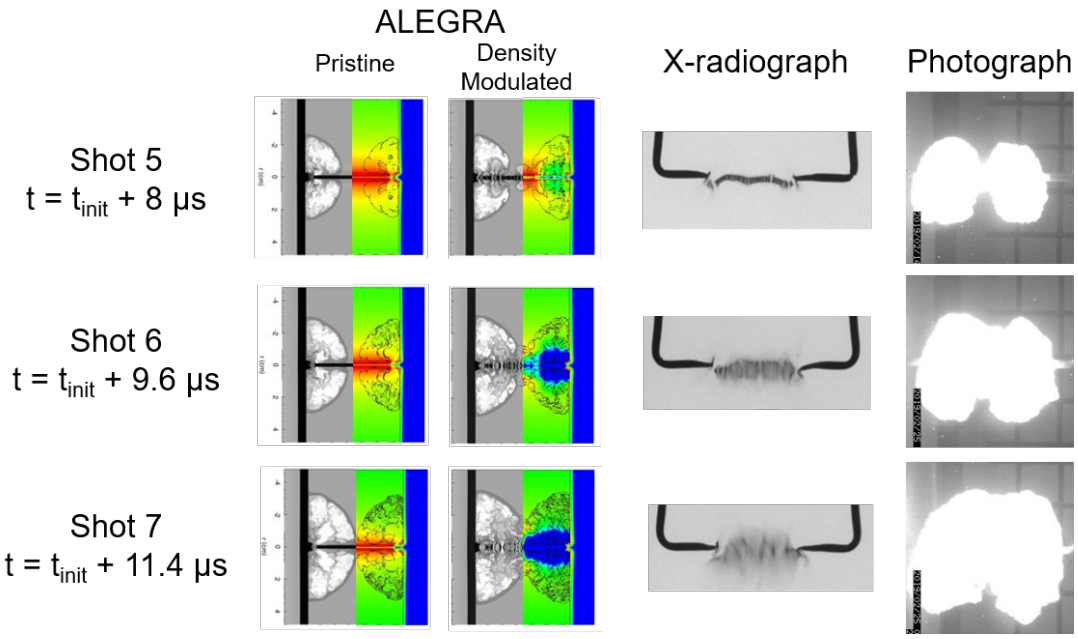

Fig. 3 Comparison of simulations (illustrating density [grayscale] and magnetic field [color]), X-radiography, and photography of exploding wires

4. Conclusion

Based on the initial calculations and proof-of-principle experiments, spatial visualization of magnetic fields using PRad is feasible and would result in information directly beneficial to Army interests, provide a unique validation tool for multiphysics codes, and probe material states in EM environments that are yet to be investigated. Key takeaways from the baseline exploding wire experiments in comparison with ALEGRA simulations are 1) the magnetic field is sensitive to the finite details of the material state, the material distribution, and conduction pathways inside the interaction zone, and 2) the experimental design will allow us to probe these states. Thus the addition of a capability to directly observe and compare the magnetic field in situ would provide the opportunity to greatly improve confidence in MHD codes and relevant material models, while also allowing identification of exactly where the current is flowing in complex pulsed power experiments.

5. References

1. Robinson A, Brunner T, Carroll S, and coauthors. ALEGRA: an arbitrary Lagrangian-Eulerian multimaterial, multi-physics code. Proceedings of the 46th AIAA Aerospace Sciences Meeting; 2008. AIAA-2008-1235.

2. Noble C. Anderson A, Barton N, Bramwell J, Capps A, Chang M, Chou J, Dawson D, Diana E, Dunn T, et al. ALE3D: an arbitrary Lagrangian-Eulerian multi-physics code. Livermore (CA): Lawrence Livermore National Laboratory (LLNL); 2017 May 23. Report No.: LLNL-TR-732040.

3. Chace WG, Moore HK, editors. Exploding wires. Boston (MA): Springer; 1968.

4. Barbaglia M, Prieto, G. Electrical behavior of exploding copper wire in ambient air. Physics of Plasmas. 2018;25:072108.

5. Zellner M, Uhlig W. Implementation of a point spread function method to analyze flash radiography images: Image enhancement, movie generation, and projection detangling. In progress.

Appendix A. Example Exploding Wire Experiments

This appendix describes a set of three experiments in which copper wires were exploded via capacitive electrical discharge. The experiments are labeled Shots 5, 6, and 7, which refers to their logging in a US Army Combat Capabilities Development Command Army Research Laboratory (ARL) notebook. In all cases, the load wire was made to be as similar as possible so the set of experiments could be self-compared. The experiments were characterized using high-speed photography and X-radiography to observe the overall event, photon Doppler velocimetry (PDV) to characterize the wire expansion, high-voltage probes at the electrical contacts of the wire, and a Rogowski current probe to assess the electrical circuit. In addition, still photography and witness materials were employed to convey an assessment of the mechanical forces involved to evaluate any potential damage within a PRad vessel.

The copper wires were constructed by hand using a layered tube approach to thicken a central solid-core wire. Figure A-1 is a photograph of the design. Important aspects included a linear section designed to explode that fits within the PRad Identity lens field of view (~35-mm straight copper wire with a diameter of 1.6 mm tapered up to 4.0 mm at each end over approximately 15 mm in length), capability to carry currents near 200 kA prior to and during the dynamic event, tapering of the wire radius when transitioning from thick to thin regions to reduce induced explosion points, and an overall geometry to complement PRad's coupling to the magnetic field (magnetic field orthogonal to the proton propagation direction for regions of interest, and aligned elsewhere).

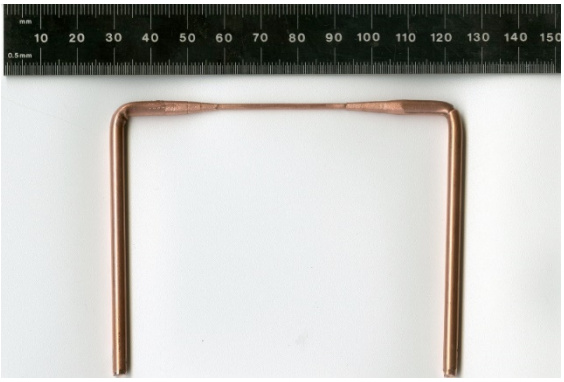

Fig. A-1 Copper wire that was exploded via capacitive electrical discharge (Shot 7)

Figure A-2 shows the general experimental setup used to explode the wires, including the energy storage capacitor, a spark-gap switch, low-inductance leads, low-inductance PRad vessel feedthrough simulant, wire mounting hardware, and supporting diagnostics. Setup also included a Shimadzu HPV-X2 overlooking the experiments from a viewpoint slightly above but in line with the X-ray source, and a Photron SA5 that provided a global view.

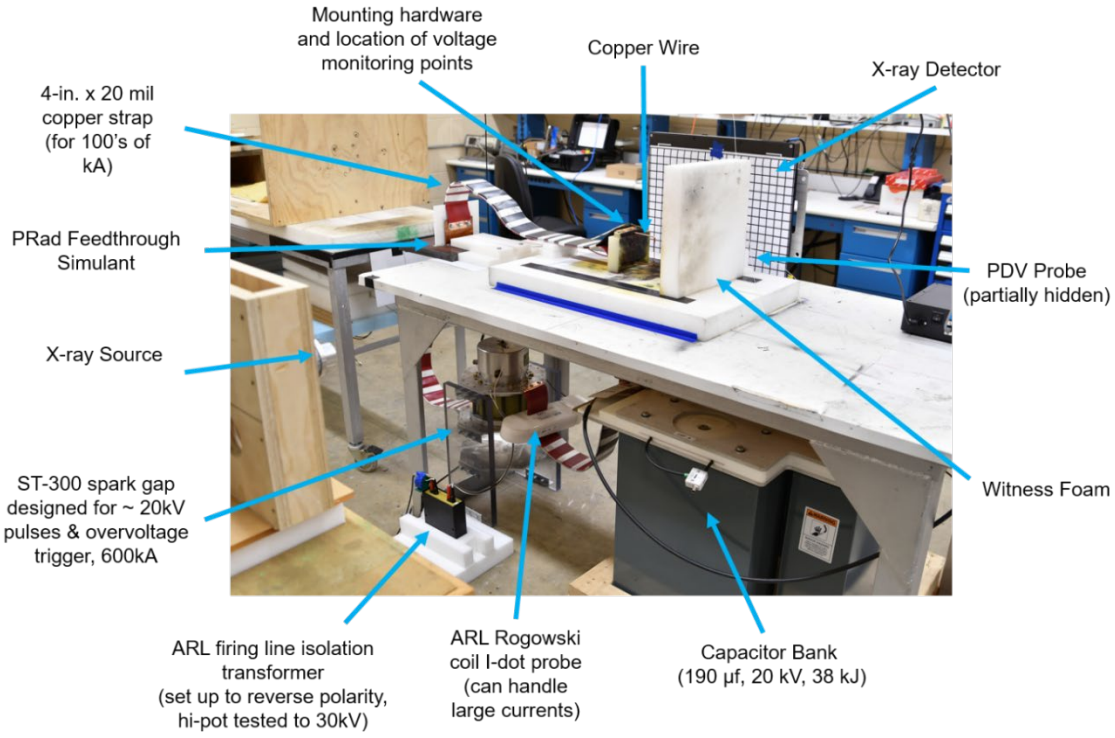

Fig. A-2 Setup used to explode a wire via capacitive electrical discharge

The Shimadzu recorded the experiments over 256 frames collected at 5,000,000 fps. It used a "start" trigger initiated from a current monitor attached to the firing line isolation transformer (defined as t = 0) and was equipped with a Nikon 80-400 lens set to 140 mm and a 12.7-mm extension between camera and lens. The camera also used two 8-stop neutral density filters and an aperture setting of f32. The Photron camera recorded the experiments using 10,000 fps paired with a 370-ns shutter. The Photron recorded for greater than 1.5 s and utilized a "center" trigger to capture ample durations before and after each experiment. The camera was equipped with a Nikon 50-mm lens and used an aperture setting of f1.4. A single X-radiograph of the event was collected at a presubscribed time relative to t = 0. The radiography used a single L-3 Pulse Sciences 150-kV system source configured with a soft X-ray tube to lower the output photon energy. The radiograph was collected using a Carestream HPX-DR DRX Plus detector. A single point of PDV was collected from each experiment monitoring the wire's radial expansion. The expansion was monitored at an angle of 45° in the direction in which the induced Lorentz force would propel the particles. This diagnostic was set to record using a start trigger (begin at t = 0) and record velocities up to 10 km/s.

Figure A-3 shows the current within the circuit, and Fig. A-4 shows the voltage traces recorded across the wire load of the exploding wire experiments. The current was attained by numerically integrating the signal from a calibrated Rogowski coil.

The charging voltage on the capacitor bank was set to 15 kV for a total system energy of 21.5 kJ. With this setup the peak current averaged 207 ± 2 kA over the three experiments. A fit to the current data using an inductive-resistive-capacitive model yielded an inductance between 700 and 720 nH for the three shots. An inflection in the current trace around 24 μs indicates a change in the electrical response. The voltage trace along with the high-speed video and X-ray give further insight to the process. There are two major inflections followed by a peak and then rapid drop-off. The first inflection in voltage indicates a rise in electrical resistance and begins when ends of the narrow piece of wire (1.6-mm section) begin to blow (16.5, 19.1, and 18.4 μs for Shots 5, 6, and 7, respectively). This is followed by the majority of wire beginning to melt and the ends of blown wire continuing to expand, resulting in a continued "slow" rise in resistance. At the second inflection, initiation of vaporization along the entire wire begins resulting in a rapid increase in resistance (23.0, 22.4, and 22.5 μs for Shots 5, 6, and 7, respectively). This voltage and thus resistance peaks (24.4, 24.3, and 23.5 μs) are followed by a rapid decrease, indicating that the plasm has connected along the entire wire, forming a complete low-impedance channel. Due to losses in the internal resistance of the capacitors and inductance of the leads, the actual energy supplied to the mount and wire is approximately 14–15 kJ.

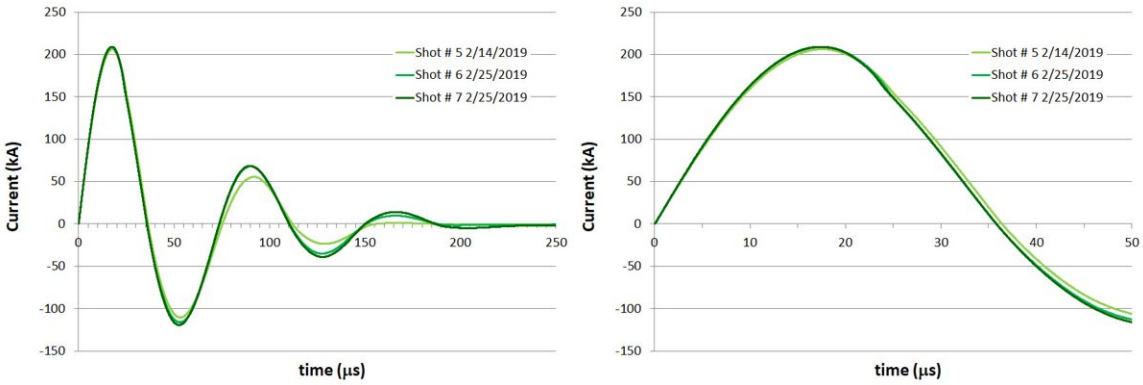

Fig. A-3 Current traces from the three exploding wire experiments

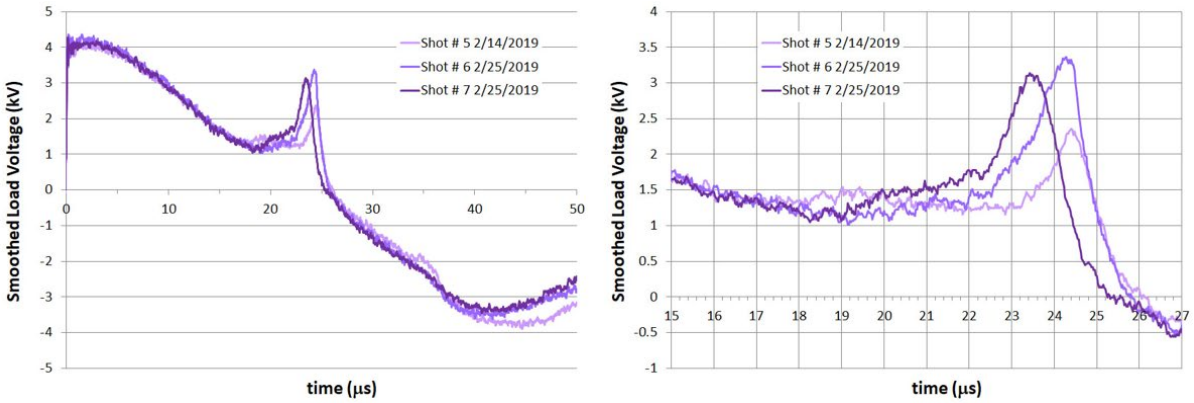

Fig. A-4 Voltage traces from the three exploding wire experiments

Figure A-5 shows photography of the Shot 5 event captured by the Shimadzu HPV-X2 camera. From these data it is evident that the wire begins to explode near the ends of the straight section at the joints with the conical tapers (t = 16.66 μs). The onset of light in the photography correlates well with the slight rise in the voltage monitor described. However, PDV signals shown in Figs. A-6 and A-7 indicate that the center of the wire began slow movement earlier in time (detectible movement by t = 8 μs). This may be due to the wire bending under the influence of the Lorentz force or could be thermal expansion. Near t =16.6 μs the PDV signal detects the initiation of wire explosion as vibrations and loss in continuity of signal, which correlates well with the optical and electrical monitors. Near t = 21–25 μs the PDV signal indicates a significant uptick in the particle velocities. Correlation with optical photography suggests that this is the expansion of material along the length of the wire. PDV indicates that peak particle velocities near 1800 m/s and expansion occurs through 400 μs.

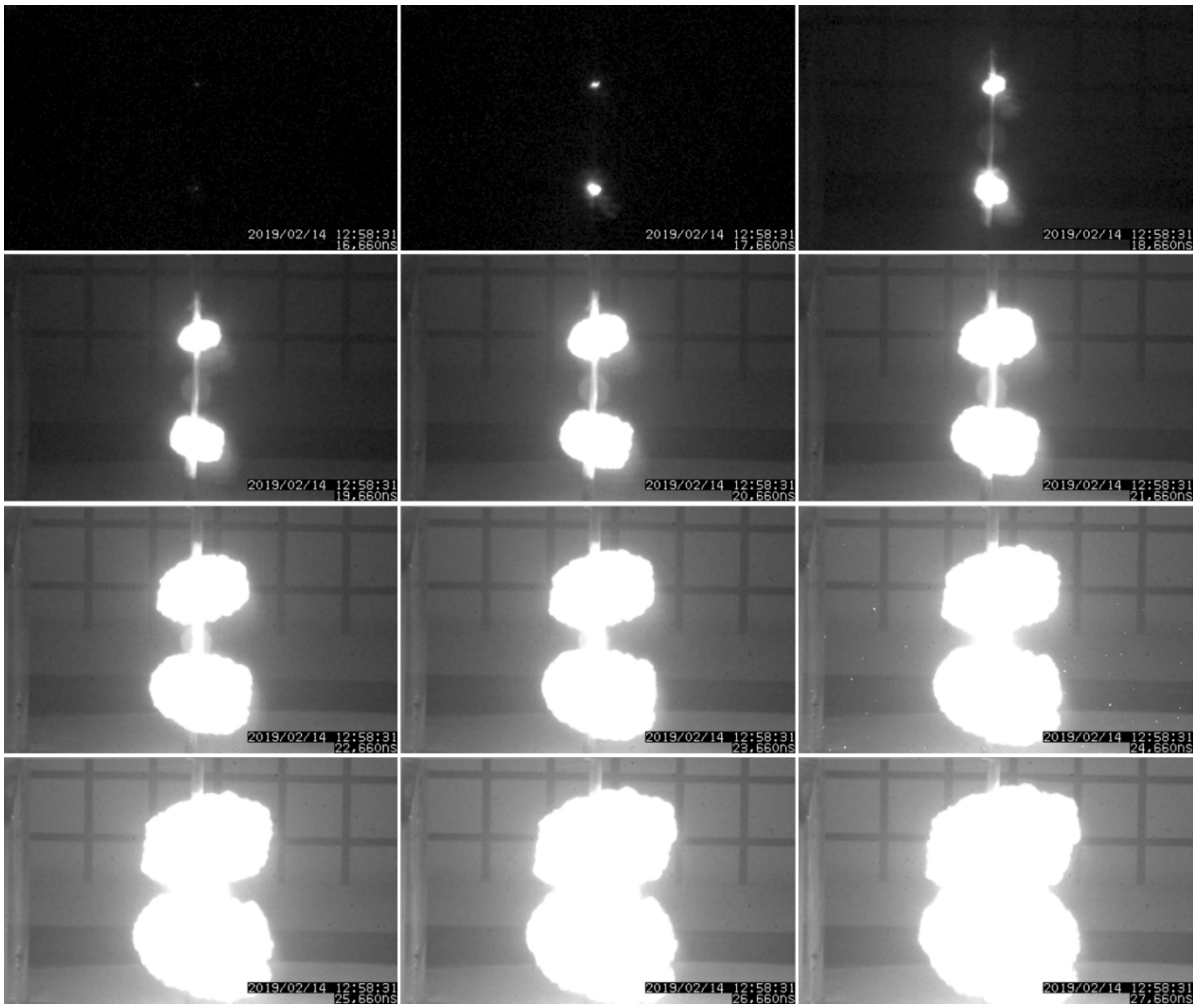

Fig. A-5 High-speed optical photography of the Shot 5 exploding wire experiment. Images display snapshots at 1.0-µs intervals beginning at t = 16.66 µs.

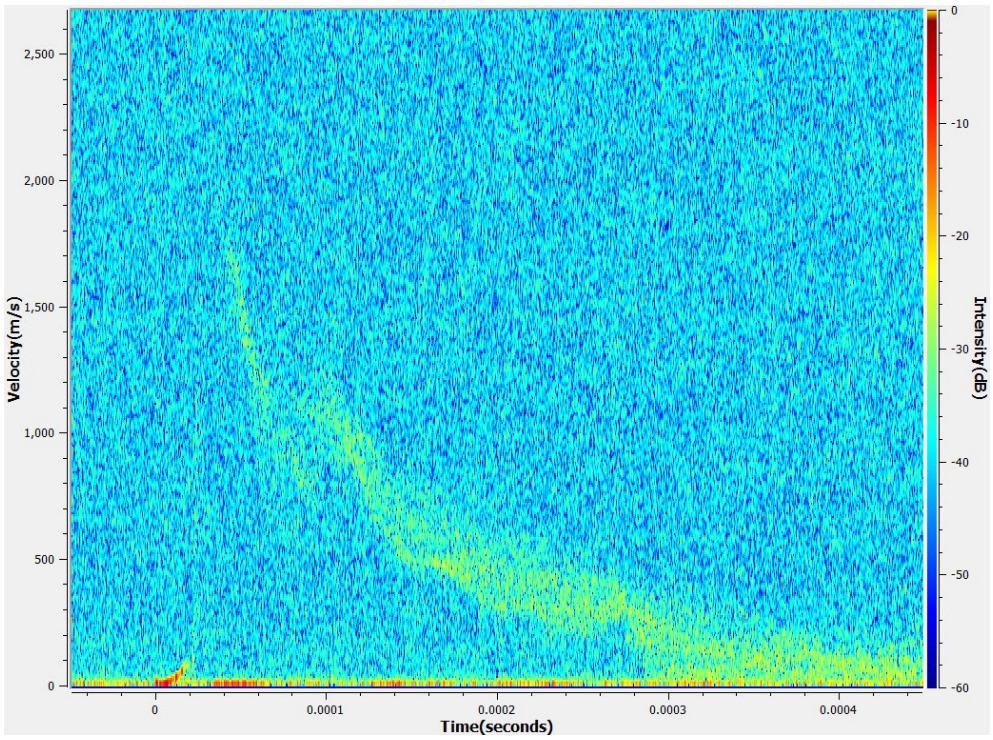

Fig. A-6 Spectrogram depicting PDV-measured expanding wire particle velocities

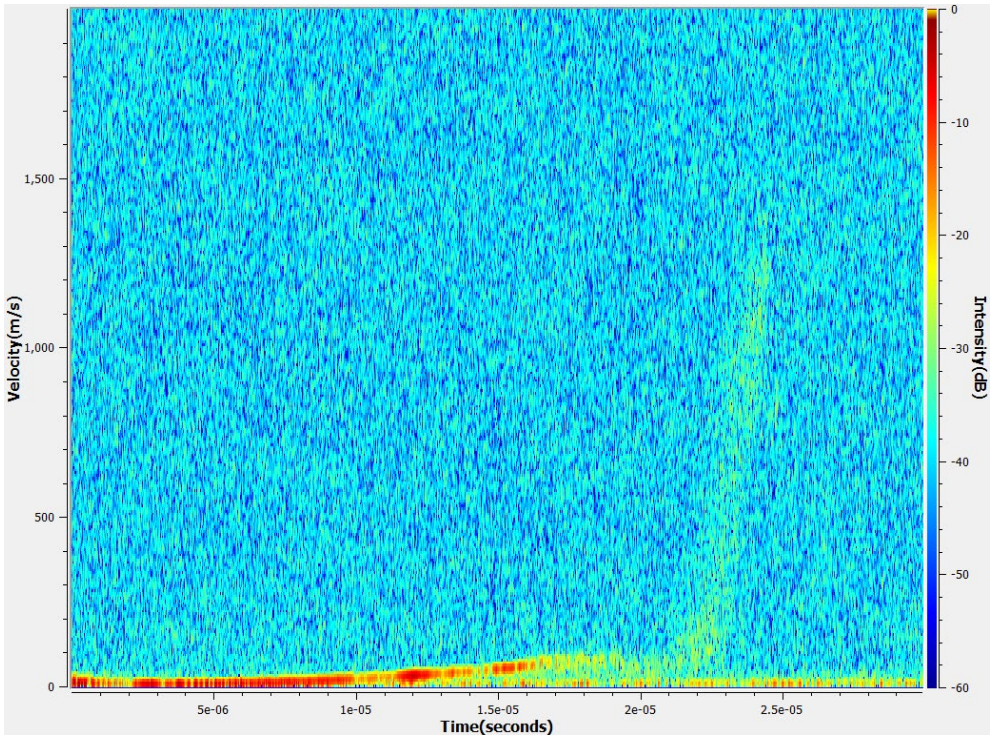

Fig. A-7 Spectrogram depicting velocities of the exploding wire measured by PDV, focusing on the early-time feature dynamics

Figure A-8 shows a temporal comparison of compiled experiments as viewed with X-radiography and optical photography throughout the dynamic event. From this image it becomes clear that the explosion is very asymmetric and results in a region of particles and vapor with varying average densities. The optical photography highlights a significantly expanded outer envelope in which the event is contained, while the radiography is useful to define regions of dense particles and material, indicating texture throughout the region. The radiography also indicates influence of the Lorentz force on the particles resulting from the geometry used, which pushes the particles slightly away from the initial wire position. Note that the circuit monitors indicate full conduction throughout this duration.

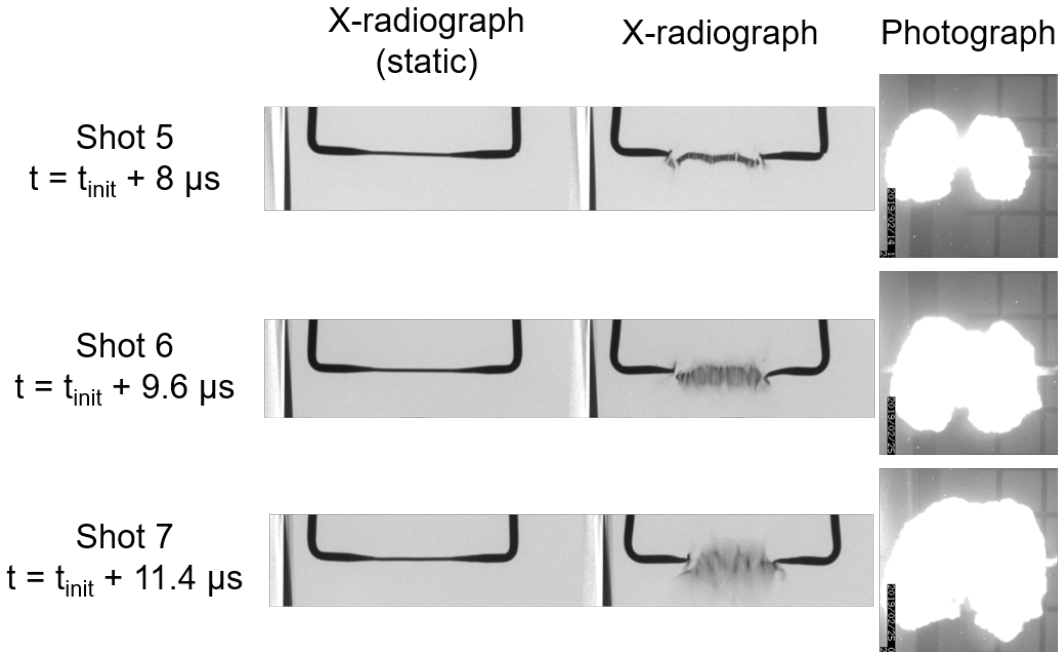

Fig. A-8 Uniformly scaled X-radiography and high-speed optical photography from three independent (but similar) experiments

Figure A-9 shows before and after photographs assessing the global influence an exploding wire exerts on its local surroundings. The geometry of the setup is such that Lorentz forces propel material outward in the plane of the wire. Therefore, the greatest risk for fragment projection will be in the plane perpendicular to the surface of the table on which the experiment is conducted. Some heuristic observations made after the experiment include the following:

1) The foam block with 0.0625-m^2 surface area weighing 450 g (direction complementing Lorentz force) propelled 0.5 m.

2) The lower copper lead punctured through 2-mm-thick Kydex and embedded approximately 20 mm into 9LB polyethylene foam sheet.

3) The upper copper lead broke off and was found lying on the floor approximately 2 m away after rebounding off a cover structure approximately 2 m above the table.

4) The paper scale screen located approximately 0.25 m away, but not within the plane influenced by Lorentz forces, remained unscathed.

5) Painter's tape was sufficient to retain the experiment in place from global motion.

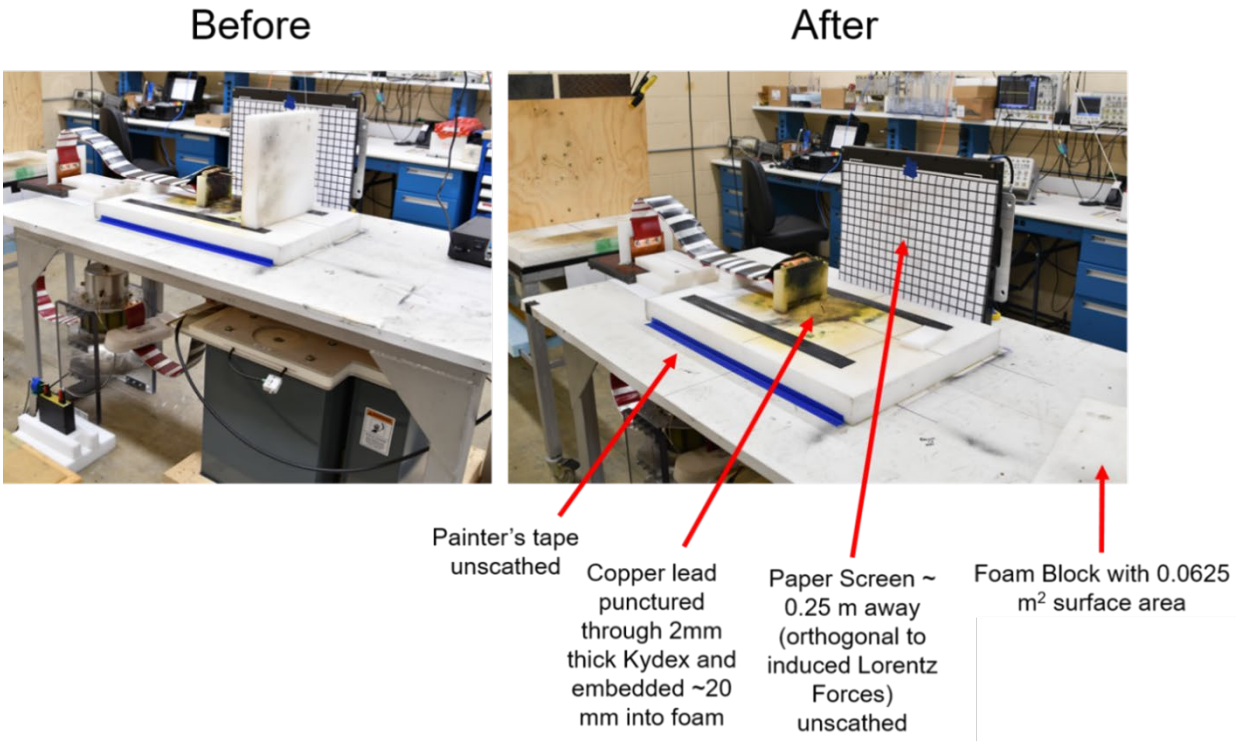

Fig. A-9 Before (left) and after (right) photographs depicting global influence an exploding wire has on the local environment

Appendix B. Example Exploding Wire Simulation Conducted using ALEGRA Multiphysics Code

We use the 2019 release (v. 7.4) of Sandia National Laboratories' MHD (magnetohydrodynamic) code, ALEGRA, to simulate several 2-D axisymmetric exploding wires. Current inflow is generated through an external resistor-inductor-capacitor circuit that couples to an anode and cathode in the computational domain. These plates are bridged by a copper wire with a diameter of 1.6 mm positioned at the axis of symmetry. The wire is connected to larger diameter wires via tapered sections to help minimize explosions at sharp corners due to localized Joule heating. The computational mesh adds dynamic inductance and resistance, thus the circuit elements are adjusted to capture the early *di/dt* that is consistent with experiment (usually 15–25 kA/μs).

Figure B-1 illustrates the current density (left colored plot), magnetic field (right colored plot), and density (grayscale plots) for a perfect wire and one with a 1% uniform distribution of densities about the mean or reference value. These images show the progression of current diffusion, wire heating, and wire explosion in a case similar to Experiments 5–7 described in the main text. Exploding wire dynamics are very sensitive to wire radius: time to melt varies as r^4/i^2. For wires with a very small diameter—up to hundreds of microns—even simulated pristine wires explode at these current levels (100–200 kA). However, at this larger diameter, the introduction of a reasonable statistical variability was necessary to induce wire explosion along its length. Additional diagnostics for the simulation (not pictured) include a Lagrangian tracer particle at $z=0$—just inside the wire surface—and radial line queries that plot velocity, temperature, density, magnetic field, and electrical conductivity as functions of time and radius. Many other time histories of global and material variables are available for inspection.

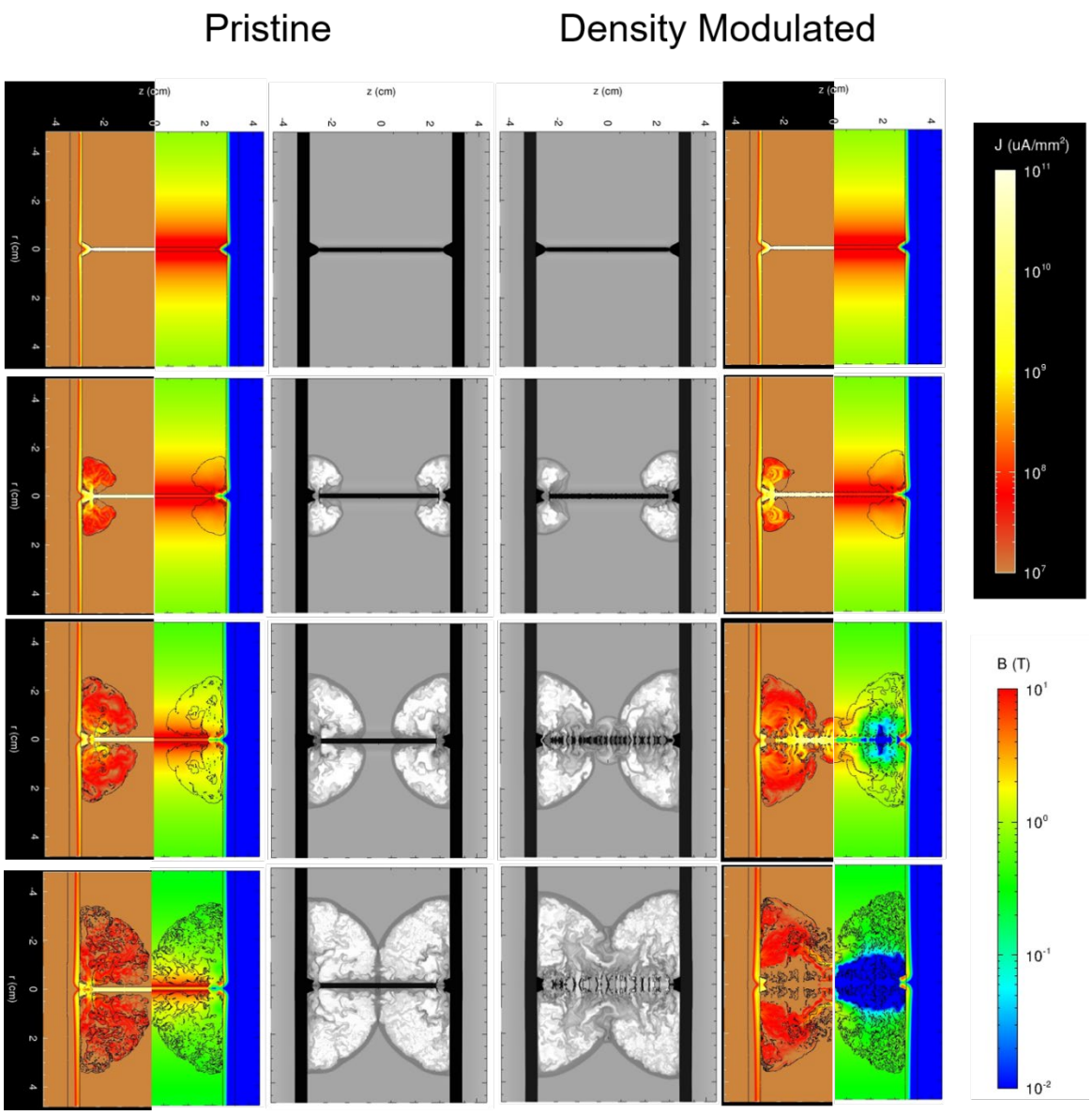

Fig. B-1 Current density (left colored plot), magnetic field (right colored plot), and density (grayscale plots) for a perfect wire and one with a 1% uniform distribution of densities about the mean or reference value

These data show magnetic field strengths reaching about 50 T at the wire surface. Also evident are the initial explosions occurring where the thin wire meets the tapered section. It explodes at this angle because of the localized heating angle and the reduced diameter. Later along the wire's length, a competition between thermal expansion, Lorentz forces, and pinching—induced by wire variability—leads to explosions where the necking is more pronounced than wider-diameter regions. Electric current is carried away by the radial expanding, conductive, low-density copper plasma.

Figures B-2 and B-3 display such a simulation at 18.5 and 22.25 μs, respectively. Visualized is the electrical conductivity (left half), density (right half), contours of enclosed current, and global tallies of the current and voltage across the computational domain. These traces match the experimental results quite well and showcase the importance of electrical conductivity models to current pathways and bulk dynamics in these extreme environments.

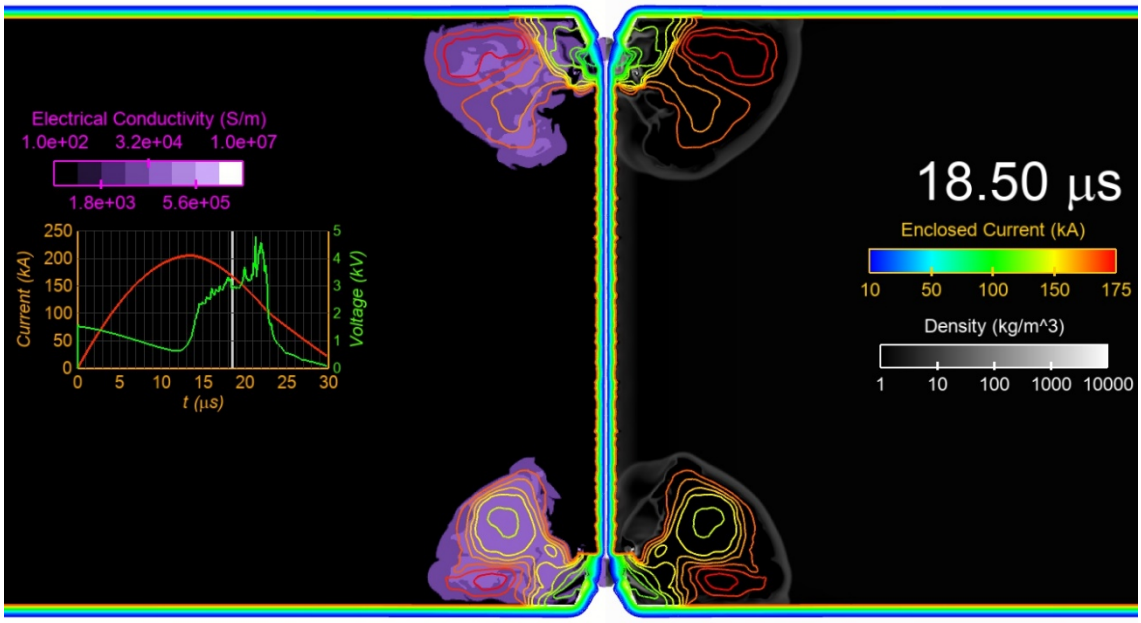

Fig. B-2 Density-perturbed simulation at 18.5 μs showing the electrical conductivity (left half), density (right half), contours of enclosed current, and global tallies of the current and voltage across the computational domain

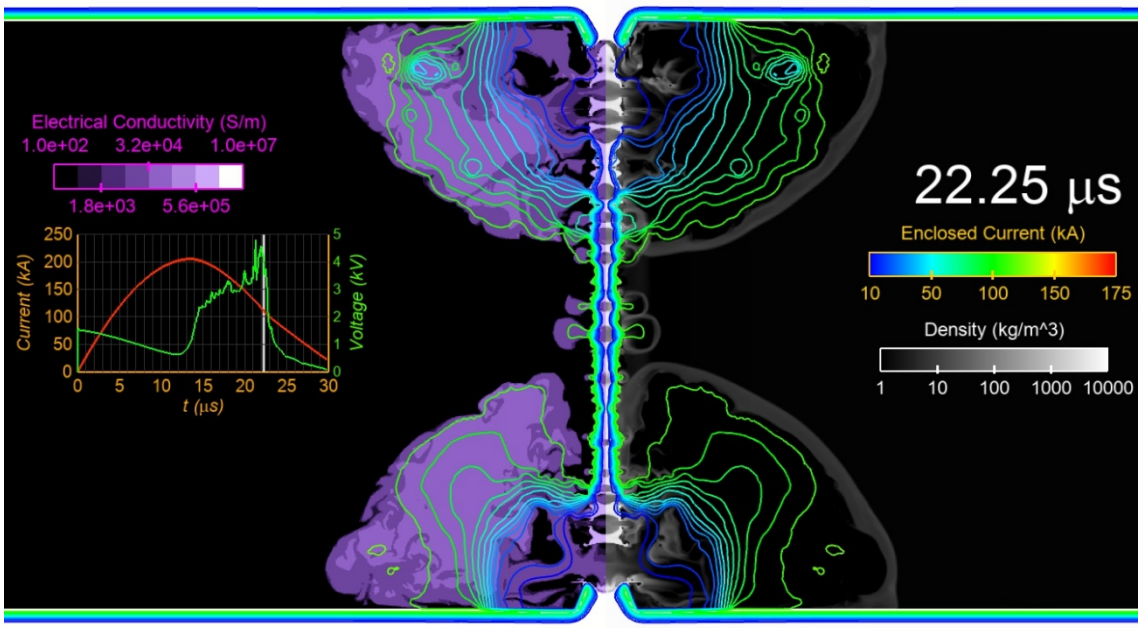

Fig. B-3 Density-perturbed simulation at 22.25 μs, showing the electrical conductivity (left half), density (right half), contours of enclosed current, and global tallies of the current and voltage across the computational domain

List of Symbols, Abbreviations, and Acronyms

2-D	two-dimensional
ARL	US Army Combat Capabilities Development Command Army Research Laboratory
EM	EM
MHD	magnetohydrodynamic
PDV	photon Doppler velocimetry
PRad	proton radiography

1 (PDF) DEFENSE TECHNICAL INFORMATION CTR DTIC OCA

2 (PDF) CCDC ARL IMAL HRA RECORDS MGMT FCDD RLD CL TECH LIB

1 (PDF) GOVT PRINTG OFC A MALHOTRA

1 (PDF) PEO CS CSS SFAE CSS FP H D BOCK

1 (PDF) PROJECT DIRECTOR SFAE GCS M E BARSHAW

2 (PDF) PM ABRAMS SFAE GCS HBCT S J ROWE R NICOL

2 (PDF) PM BFVS SFAE GCSS BV D SPENCER LTC DEAN

2 (PDF) PM GCS SFAE GCSS W BCT M RYZYI T HOWIE

1 (PDF) USMC A PURTELL C/O B SWEDISH

1 (PDF) DEPT OF THE ARMY TACOM ARDEC S CHICO

3 (PDF) DEPT OF THE ARMY TACOM AMSTA TR R C FILAR R RICKERT A LEE

1 (PDF) DEPT OF THE ARMY ABERDEEN TEST CENTER CSTE DTC AT SL V D BLANKENBILLER

11 (PDF) SANDIA NATIONAL LABORATORIES J NIEDERHAUS G HANSEN S BOVA C SIEFERT C GARASI D MCGREGOR A PORWITKZY K COCHRANE A ROBINSON J WILKES AL RODRIGUEZ

100 (PDF) CCDC ARL FCDD RLW M B LOVE FCDD RLW MA J LA SCALA D O'BRIEN FCDD RLW MB G GAZONAS FCDD RLW MD B CHEESEMAN K CHO FCDD RLW ME M KORNECKI R BRENNAN V BLAIR S KILCZEWSKI J LASALVIA P PATEL J SWAB L VARGAS-GONZALEZ FCDD RLW MG J LENHART K MASSER FCDD RLW LB F DELUCIA T JENKINS B RICE FCDD RLW LC K MCNESBY T PIEHLER B ROOS G SUTHERLAND FCDD RLW LH J ANGEL T EHLERS E KENNEDY L MAGNESS C MEYER J NEWILL B SCHUSTER B SORENSEN R SUMMERS

FCDD RLW P
D LYON
J HOGGE
T VONG
FCDD RLW PA
J BALL
P BERNING
S BILYK
J CAZAMIAS
M COPPINGER
J FLENIKEN
T KOTTKE
G THOMSON
W UHLIG
A VALENZUELA
L VANDERHOEF
C WOLFE
B WILMER
FCDD RLW PB
C HOPPEL
S SATAPATHY
S WOZNIAK
FCDD RLW PC
R BECKER
T BJERKE
D CASEM
J CLAYTON
R LEAVY
S SEGLETES
A SOKOLOW
A TONGE
C WILLIAMS
FCDD RLW PD
A BARD
N BRUCHEY
R DONEY
M DUFFY
S HALSEY
M KEELE
D KLEPONIS
R MUDD
F MURPHY
D PETTY
C RANDOW
J RUNYEON
S SCHRAML
K STOFFEL
G VUNNI
V WAGONER
M ZELLNER
FCDD RLW PE
B AYDELOTTE
P BARTKOWSKI
M BURKINS
D GALLARDY
P GILLICH
D HORNBAKER
J HOUSKAMP
T JONES
C KRAUTHAUSER
M LOVE
K MCNAB
P SWOBODA
FCDD RLW PF
N GNIAZDOWSKI
S HUG
C CUMMINS
D ERDMAN
R KARGUS
FCDD RLW PG
D HOFSTETTER
B HOMAN
S KUKUCK
C PECORA
J STEWART
FCDD RLW S
J CIEZAK-JENKINS